CFD Letters

Journal homepage:
https://semarakilmu.com.my/journals/index.php/CFD_Letters/index
ISSN: 2180-1363

Comparative Analysis on the Effect of Bow Shapes on the Ship Resistance using CFD Simulation and Model Test

Mohammad Ridwan Utina[1,2 *], I Made Ariana [1,] Dian Purnamasari[2]

[1] Department of Marine Engineering, Faculty of Marine Technology, Institut Teknologi Sepuluh Nopember, Surabaya, Indonesia
[2] Research Center for Hydrodynamic Technology, The National Research and Innovation Agency (BRIN), Surabaya, Indonesia

ARTICLE INFO

Article history:
Received 6 May 2024
Received in revised form 8 June 2024
Accepted 9 July 2024
Available online 31 October 2024

Keywords:
Axe bow; conventional bow; bow shape, reduction; total resistance; residuary resistance; friction resistance; CFD; model test

ABSTRACT

Shipping companies and ship owners are very concerned with reducing operating costs. One way to achieve this is by improving the hydrodynamic performance of ships, which can reduce fuel consumption by decreasing total resistance. Optimizing ship design, particularly the bow shape, is crucial for enhancing hydrodynamic performance, fuel efficiency, and operational costs. While CFD simulations have become a powerful tool in naval architecture, their accuracy and reliability in predicting hydrodynamic resistance for different bow shapes need validation through experimental data. This study employs computational tools using Fine/Marine NUMECA and model tests carried out in a towing tank. The primary objective is to compare the hydrodynamic resistance of axe bow and conventional bow shapes. Additionally, the contributions of different resistance components (residuary and friction) to each bow shape are identified and quantified. The study concludes that the axe bow shape offers notable improvements in reducing total resistance compared to the conventional bow, providing a reduction of up to 12.5%. Moreover, the residuary resistance component has a more significant effect on total resistance compared to friction resistance.

1. Introduction

The need to decrease energy usage must be extended to all sectors, including marine transportation. Shipping is the main element of it. Like any other industry, the shipping industry relies on fuel and is influenced by the instability of oil prices [1]. The international shipping sector has been significantly impacted in recent years by volatile fuel costs and more stringent emissions standards imposed by the International Marine Organization (IMO) [2]. The escalating cost of heavy fuel oil has prompted much study on fuel consumption efficiency.

The fuel cost is often the most significant expenditure in shipping operations, accounting for around 50–60% of the total operating costs [3]. As a result, shipping firms, charterers, and ship owners have been seeking methods to minimize and streamline fuel use. Minimizing ship fuel consumption is crucial for enhancing ship efficiency. It can be approached from two perspectives:

* *Corresponding author.*
E-mail address: muha009@brin.go.id (Mohammad Ridwan Utina)

https://doi.org/10.37934/cfdl.17.3.3651

minimizing the operational expenses of ships by controlling speed and optimizing routes, or by optimizing ship hull elements such as the hull, propeller, and rudder [4]. The optimization of ship performance and the reduction of resistance are topics of great interest to several academics. An alternate design is one effective method to decrease drag [5].

The efficiency of fuel consumption in vessels may be influenced by many factors, such as weather conditions, mainly wave conditions, ship speed, draft, displacement, hull shape, and propellers, which have been the focus of many studies due to the increasing fuel cost and environmental concerns [6]. The maritime world increasingly acknowledges that hull form optimization is an important aspect to be considered in the field of ship hydrodynamics in order to increase ship energy efficiency. Ship owners should evaluate the hull shape to improve their fuel economy [7]. The ship's hull shape is a crucial feature that requires careful consideration while designing the hull lines to minimize the ship's overall resistance [8]**.**

Several innovative bow hull optimizations have been developed to reduce wave-making resistance, such as the x bow [9], ax bow [10], and axe bow [11]. These designs feature sharper bow entrances and significant changes to the bow shape, with a deep and nearly vertical V-shaped section. The axe bow, in particular, is a successful concept that has proven effective in optimizing hydrodynamic resistance and seakeeping.

Hydrodynamic optimization is a crucial element in the ship design process. This optimization begins at the initial and early stages of design and continues through to the later stages and final design. Computational fluid dynamics (CFD) simulations and model test techniques are commonly used to assess hydrodynamic performance during this process [12]. Many studies have documented the use of CFD modeling in optimizing hull shapes to minimize resistance in calm water [13], examining effects on wave-making resistance [14], the impact of trim [15], hull roughness on resistance [16], and the interaction between the propeller system and the flow around the hull [17].

The purpose of this research is to investigate the hydrodynamic performance of bow hull forms in relation to the reduction of total ship resistance by comparing the axe bow shape with the conventional bow shape of fast monohulls. The two hull forms are examined under calm water conditions and various Froude numbers. Moreover, the analysis is conducted based on the individual contributions of each resistance component.

Keuning *et al.,* [18] have conducted a calm water model test of the Axe Bow Concept (ABC) and compared it with the Enlarge Ship Concept (ESC) and Wave Piercing Concept (WPC). The results show that the resistance between the three designs depends on the speed range under consideration. At ship speeds below 35 knots, the ESC has a higher resistance when compared with the ABC. Above 35 knots, this is reversed. It was found that the axe bow concept has illustrated remarkable achievement with a 30% reduction in the required installed power to sustain a design speed of 25 knots compared to the ESC, which has a conventional bow shape.

Mosaad *et al.,* [19] have also carried out a simulation by using the X-bow shape of the original DTMB 5415 model, compared with the X-bow, and found that at low Froude numbers, there is a considerable decrease in wave-making resistance of about 18%. The reduction of the intermediate Froude number changed from 22% to 30% with increased hull speed.

Similarly, Basil *et al.,* [20] have observed a simulation of fishing trawling, and the results indicate that the optimal design of the x-bow hull resulted in a resistance reduction of 4% at operational speeds and a remarkable 11% resistance reduction at trawling speeds. This result of the x-bow shape highlights its significant potential and promise compared with conventional bow shapes in reducing resistance and improving fuel efficiency.

Previous research has often focused on either experimental methods or simulations independently, lacking a comprehensive approach that combines both. This leaves a gap in validating CFD results with experimental data, particularly for innovative bow designs like the axe bow compared to conventional bows. By conducting a comparative analysis of different bow shapes using both CFD simulations and physical model tests, this study aims to provide a more accurate and validated understanding of hydrodynamic resistance. This is crucial for the design and optimization of fast patrol boats, where reducing resistance can lead to significant improvements in fuel efficiency, operational range, and speed capabilities. The findings can aid naval architects in making informed decisions about bow designs, contributing to more efficient and sustainable shipbuilding practices. This paper discusses the investigation into the influence of using the axe bow shape on a fast patrol boat's total ship resistance, residuary resistance, and friction resistance compared to a conventional bow shape. Additionally, a detailed analysis of the divergent wave and transverse wave patterns generated by both bow shapes may affect the total wave resistance. To gain a preliminary understanding of the hydrodynamic performance, a detailed analysis from a low Froude number of 0.25 to a high Froude number of 1.25 was simulated, and model test studies on both bow hull forms were conducted in calm water.

2. Methodology

2.1 Ship Geometry

The principal dimensions of the two fast patrol boats are presented in Table 1, and their geometry is shown in Figure 1.

Table 1
Principle characteristic of conventional bow and axe bow

Dimension Parameters	Conventional Bow		Axe Bow		Unit
	Model scale	Full scale	Model scale	Full scale	
Length Over All (Loa)	4.302	60.23	4.286	60.00	m
Length Water Line (Lwl)	4.048	56.68	4.286	60.00	m
Beam (B)	0.545	7.624	0.544	7.622	m
Draft (T)	0.178	2.485	0.141	1.975	m
Volume displacement	0.125	352.6	0.126	353.1.	m^3
Wetted Surface Area	2.361	462.9	2.347	460.1	m^2

For the model test, both ships were scaled at 1:14, while full-scale models were used for numerical simulations in calm water across a range of Froude numbers from Fr = 0.25 to 1.25, corresponding to ship speeds from Vs = 12 to Vs = 59 knots. The model test, conducted to validate simulation results, was limited to speeds from Vs = 24 to Vs = 30 knots. This study employed both model testing and computational simulations to explore various aspects, including the influence of hull form and Froude number variations on total resistance..

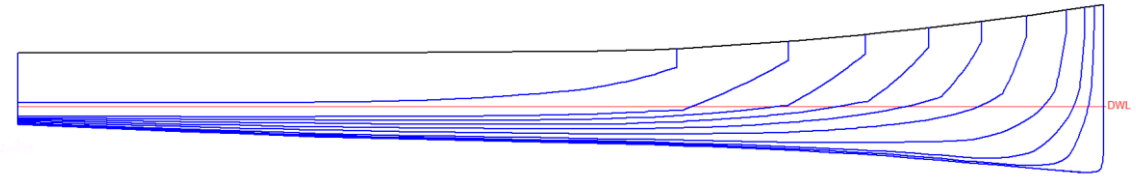

(a)

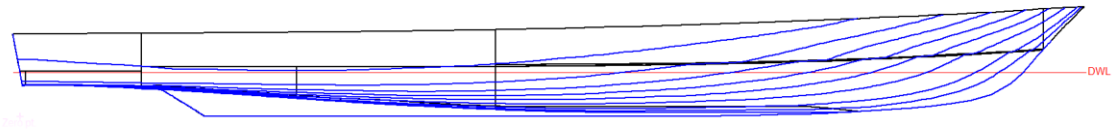

(b)

Fig. 1. Comparison of the ship profiles of axe bow (a) and conventional bow (b)

2.2 Numerical Approach

The simulations were conducted by incorporating geometric measurements into meshing, solving, and post-processing processes. A model hull was imported in para-solid format, and a mesh was produced using an unstructured hexahedral mesh generator. The simulations were conducted in calm water conditions.

2.2.1 Solver

The numerical solver used in this study is the ISIS-CFD flow solver of the NUMECA Fine/Marine. The solver is based on the finite volume method to build the spatial discretization of the transport equations to solve the incompressible unsteady Reynolds-averaged Navier–Stokes equations (RANSE). The choice of turbulence models is crucial for modeling flow fields. This study uses the Shear Stress Transport (SST) k–ω model to resolve turbulence. The SST k-ω model is effective for simulating ship hydrodynamics, provided the mesh quality meets stringent criteria. Maintaining appropriate y+ values, ensuring mesh alignment around the hull, and refining the wake region are critical steps in obtaining reliable CFD results. These measures collectively ensure that the model can accurately capture the complex interactions between the hull and the surrounding fluid, leading to precise predictions of hydrodynamic resistance [21]. The SST k–ω model provides a simpler alternative to two-equation turbulence models, improves the predictions made by algebraic mixing-length models, and builds a local model for complicated flows [22].

2.2.2 Governing equations

The governing equations of fluid flow are solved numerically. The continuity equation, sometimes known as the Navier-Stokes equation, and the energy conservation equation are the three primary equations regulating fluid flow. Because they are fundamental to all fluid computations, every CFD code implicitly solves the conservation equations of mass and momentum [23]. The spatial discretization and discretization of the transport equations were accomplished using a finite volume technique using our solver. The following are the conservation equations for mass, momentum, and volume for the incompressible flow with external forces, which can be written in tensor form in the Cartesian coordinate system and expressed in Eq. (1) and Eq. (2) as follows:

$$\frac{\partial \bar{u}_i}{\partial x_i} = 0 \tag{1}$$

$$\frac{\partial(\rho\bar{u}_i)}{\partial t} + \frac{\partial}{\partial x_i}\left(\rho\bar{u}_i\bar{u}_j + \rho\overline{u_i'u_j'}\right) = \frac{\partial \bar{p}}{\partial x_i} + \frac{\partial \bar{\tau}_{ij}}{\partial x_j} \tag{2}$$

Where u_i is the relative averaged velocity vector of flow between the fluid and the control volume, $u_i' u_j'$ is the Reynolds stresses, p is the mean pressure and τ_{ij} is the mean viscous stress tensor components for Newtonian fluid under the incompressible flow assumption, and it can be expressed in Eq. (3) as follows:

$$\bar{\tau}_{ij} = \mu \frac{\partial \bar{u}_i}{\partial x_j} + \frac{\partial \bar{u}_j}{\partial x_i} \tag{3}$$

2.2.3 Computational domain and boundary conditions

To minimize computing effort and expense, the computational domain is configured as a rectangular prism, representing just half of the ship's body. This decision was made after considering the symmetry of the hull and the fact that the ship is only traveling forward. Figure 2(a) shows methods for determining the computational domain's dimensions. According to the International Towing Tank Conference (ITTC) suggested processes for ship CFD applications, the dimensions in the (x-y-z) directions are specified as (5.0LWL-2.0LWL-2.0LWL) [24]. The ship's meshing was done using a tetrahedral approach, as shown in Figure 2(b). An unstructured surface mesh grid is used to discretize the computational domain. The mesh distributed around the ship hull consists of about 2.506 million cells.

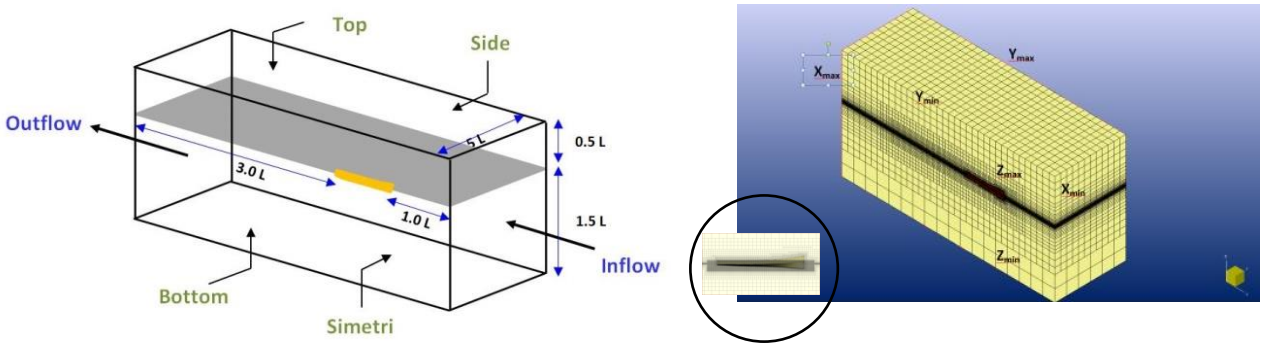

(a) (b)

Fig. 2. Computational domain (a) and (b) meshing of model

2.3 Resistance Definition

There are some methods to break down a ship's total ship resistance (RT), which is the amount of force required to keep the ship's speed constant. Based on The International Towing Tank Conference (ITTC), ship resistance in calm water can be classified into two components: friction resistance and residuary resistance. One of the dominant components of residuary resistance is wave resistance, which relates to the energy loss caused by waves created by the vessel and viscous pressure resistance.

The total resistance of a ship is comprised of two primary components: frictional resistance (R_F) and residuary resistance (R_R), as described in Eq. (4). Based on physical phenomena, ship resistance can also be divided into two subtypes: viscous resistance (R_V) and wave resistance (R_W). Viscous effects are excluded from wave resistance, which is therefore considered an inviscid phenomenon [25]. The entire hull forms a boundary layer that expands as it moves downstream. The boundary layer thickness is defined as the distance from the hull surface to the point where the velocity reaches 99% of the undisturbed flow velocity [26].

$$R_T = R_F + R_R = R_V + R_W \quad (4)$$

For non-dimensionless, the total resistance coefficient C_T is expressed as in Eq. (5) [27]:

$$C_T = \frac{R_T}{\frac{1}{2}.\rho.WSA.V_S^2} \quad (5)$$

Where R_T is the total resistance, ρ is the water density, WSA is the ship wetted surface area and V_S is the ship speed.

Then, the total resistances coefficient can be defined as :

$$C_T = C_F + C_R = C_V + C_W \quad (6)$$

C_T is the total resistances coefficient, C_F is the frictional resistances coefficient, C_R is the coefficient of residuary resistance C_V is the viscous resistances coefficient, and C_W is the wave resistance coefficient. However, residuary resistance changes due to many parameters, especially bow shape.

The frictional resistance coefficient directly relates to the ship wetted surface area and can be estimated by using the ITTC 1957 formula in Eq. (7) as follows:

$$C_F = \frac{0.075}{(\log 10R_e - 2)^2} \quad (7)$$

By using Eq. (6), the residuary resistance C_R can be derived from difference between total resistance and friction resistance.

2.4 Model Test

Ship models of conventional bow and axe bow shapes were made of wood, which was laminated with fiberglass-reinforced plastic. To mark the draft line and section line and to ensure the similarity between actual ship and ship models, an accurate measurement of model dimension is carried out in the marking table. The choice of model scale is 14, which is taken based on the capability of the towing tank facility.

The model tests were conducted in the towing tank of the Indonesian Hydrodynamic Laboratory, with a size of 220 m x 11 m x 5.5 m. A resistance dynamometer apparatus was equipped in the carriage of the towing tank. The set-up configuration test of models is directly connected to the towing carriage by resistance dynamometer apparatus so that the models can move vertically and trim, as illustrated in Figure 3. The resistance dynamometer is equipped with a load cell to measure the resistance force acting on the ship model while being towed at a certain speed. A clamp apparatus is installed to tow the model during acceleration, release it to measure the resistance, and clamp it before model deceleration. The ship model is free to move with two degrees of freedom: pitch and heave. In the test program, the models are towed in calm water with a range of model speed from Vm = 3.30 m/sec to 4.40 m/sec, which corresponds to ship speed Vs = 24 knots to Vs = 32 knots.

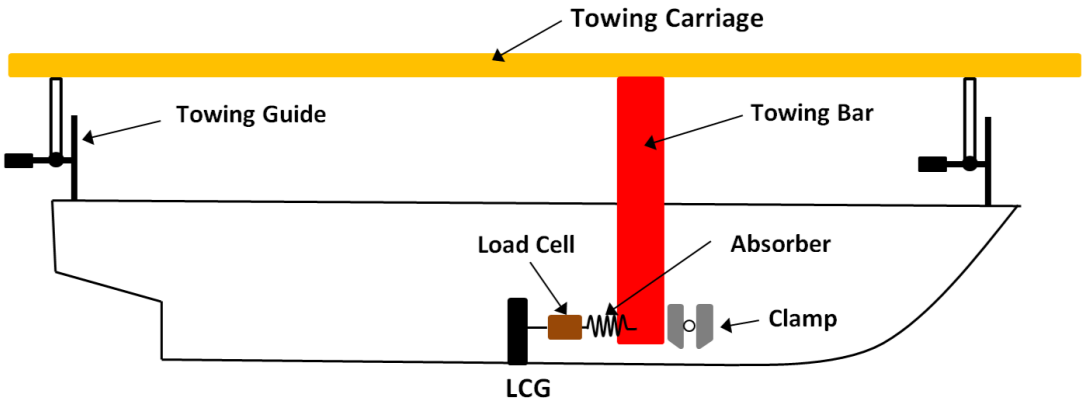

Fig. 3. A schematic diagram of towing system and set-up model test

3. Result

3.1 Validation of Total Resistance by Model Test

The generated simulation results of bow shape hulls were validated through a series of model tests conducted at the Indonesian Hydrodynamic Laboratory in Surabaya. These tests evaluated the performance of axe-bow and conventional bow shapes at model ship speeds ranging from Vm = 3.30 to Vm = 4.40 m/sec, corresponding to full-scale ship speeds of Vs = 24 to Vs = 32 knots.

As shown in Table 2 and Figure 4, there was good agreement between the total resistance results from the model tests and CFD simulations, with the percentage error not exceeding 5%.

Table 2
Percentage error of total resistance between model test and simulation CFD in (kN)

Fr	Model Test	CFD	Error
0.51	133.64	129.83	2.8%
0.55	150.64	145.87	3.2%
0.59	167.18	162.34	3.2%
0.64	182.92	179.76	1.6%

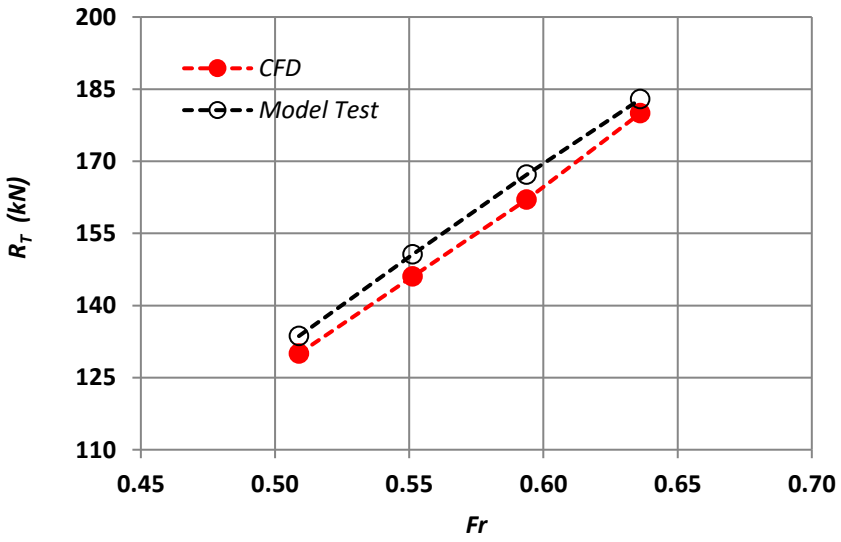

Fig. 4. Total ship resistance of simulation CFD and model test

Figure 5 presents a visualization comparing the wave patterns from the CFD simulation and the model test results. Although the comparison is not perfectly accurate, it still shows good similarities between the two visualizations. The detailed influence of bow shape on the wave pattern will be discussed in sub-section 3.2.

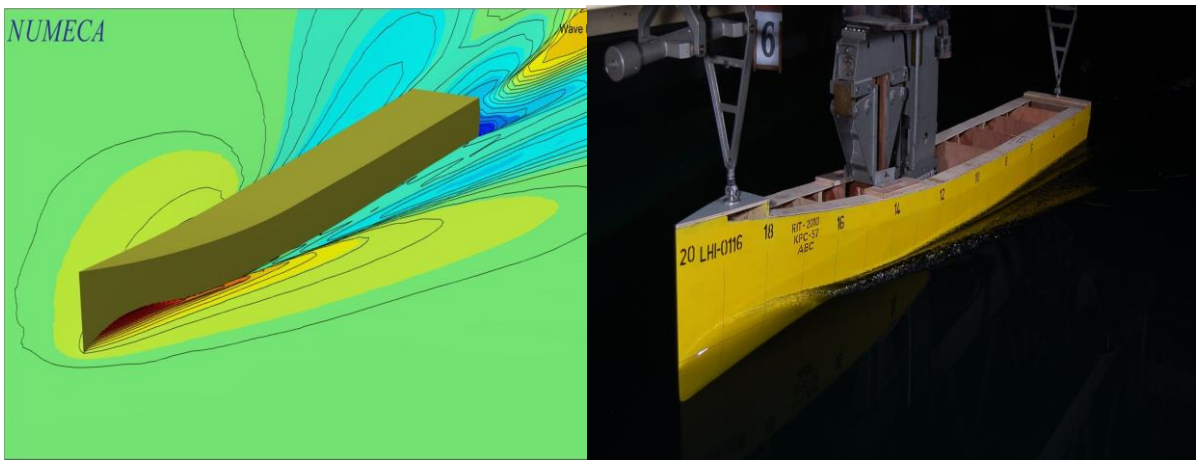

Fig. 5. Visualization of wave pattern of simulation CFD and model test at model speed Vm = 3.85 m/sec

3.2 Numerical Result

The computational investigation into predicting the total ship's resistance in calm water conditions primarily focuses on two aspects: hull form and ship speed. Simulations are executed under specific test conditions, covering only half of the hull, with results duplicated for the entire hull. The analysis explores the impact of conventional and axe-bow shapes on total resistance, providing deeper insight into hydrodynamic characteristics by quantifying residuary and friction resistances. Simulations are conducted for Froude numbers from Froude number from Fr = 0.25 to Fr = 1.25, corresponding to ship speed from Vs = 12 to Vs = 59 knots.

3.3 Effect of the Froude Number on the Total Resistance of the Ship

From the simulation, the characteristics of total ship resistance and the total ship resistance coefficient are summarized in Table 3. Figure 6 shows that the total ship resistance for both bow shapes is proportional to ship speed.

Figure 7 illustrates the presence of a hump and a hollow in the total resistance curve. It is found that at certain ship speeds, the crests of the wave systems can coincide, creating a hump in the total resistance and hollows where the crests of one system align with the troughs of another. At low Froude numbers, from Fr = 0.25 to Fr = 0.35, the total resistance coefficient decreases gradually as the Froude number increases, then increases from Fr = 0.35 to F r= 0.45, and decreases gradually again until Fr = 1.00.

The increment percentage of total resistance varies as the ship speed increases. At speeds ranging from Vs = 12 to 20 knots, the increment percentage varied significantly, between 16% and 25% for the conventional bow and between 13% and 25% for the axe bow. In contrast, at speeds from Vs = 22 to 59 knots, the increment percentage shows a similar trend for both bow shapes, ranging between 7% and 16%.

Table 3
Characteristic of total resistance and total resistance coefficient at various Froude number

Ship Speed		Conventional Bow			Axe Bow		
Knots	m/s	F_r	R_T	C_T	F_r	R_T	C_T
12	6.16	0.26	42.16	4.69	0.25	42.76	4.78
14	7.19	0.30	51.66	4.22	0.30	56.54	4.64
16	8.22	0.35	61.64	3.86	0.34	65.12	4.09
18	9.24	0.39	81.28	4.02	0.38	77.35	3.84
20	10.27	0.44	107.66	4.31	0.42	97.31	3.91
22	11.30	0.48	128.21	4.24	0.47	114.10	3.79
24	12.34	0.52	145.28	4.03	0.51	129.83	3.62
26	13.36	0.57	162.32	3.84	0.55	145.87	3.46
28	14.39	0.61	178.34	3.64	0.59	162.34	3.32
30	15.42	0.65	195.69	3.48	0.64	179.76	3.21
32	16.45	0.70	220.82	3.45	0.68	201.71	3.16
34	17.47	0.74	238.08	3.30	0.72	217.81	3.03
38	19.52	0.83	274.90	3.05	0.80	257.95	2.87
42	21.58	0.92	317.70	2.88	0.89	302.27	2.75
46	23.64	1.00	369.58	2.79	0.97	346.51	2.63
50	25.70	1.09	427.09	2.73	1.06	403.40	2.59
53	27.24	1.16	481.82	2.74	1.12	448.39	2.56
56	28.78	1.22	548.45	2.80	1.19	500.52	2.56
59	30.32	1.29	628.29	2.89	1.25	568.78	2.62

Figure 8 and 9 illustrate the residuary resistance coefficient for both conventional and axe bows, respectively, showing a similar trend to the total resistance coefficient as ship speed changes. At Froude numbers above 0.5, friction resistance becomes the dominant factor in total resistance. However, from Fr = 0.25 to 0.5, the residuary resistance coefficient of axe bow shape becomes more dominant than friction resistance in contributing to the total resistance coefficient. While conventional bow shape, the residuary resistance coefficient illustrate dominant contribution from Fr = 0.25 to 0.65.

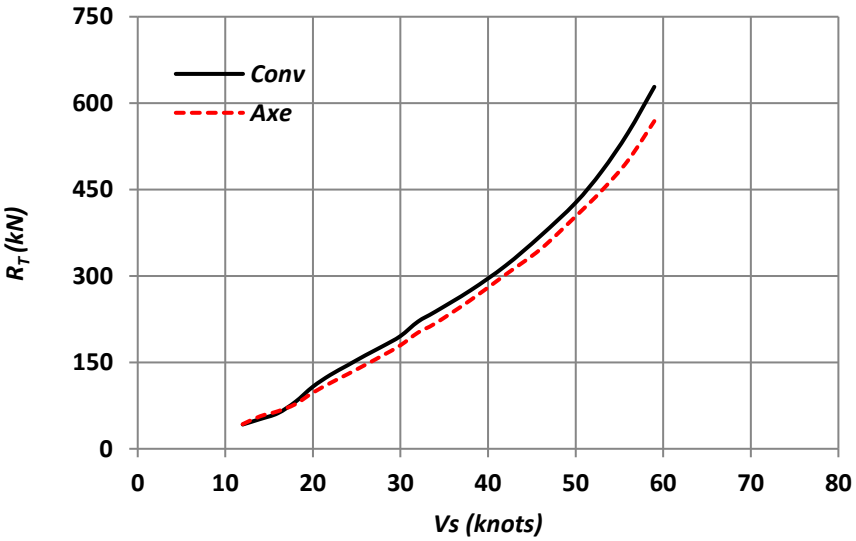

Fig. 6. Total ship resistance of conventional bow and axe bow

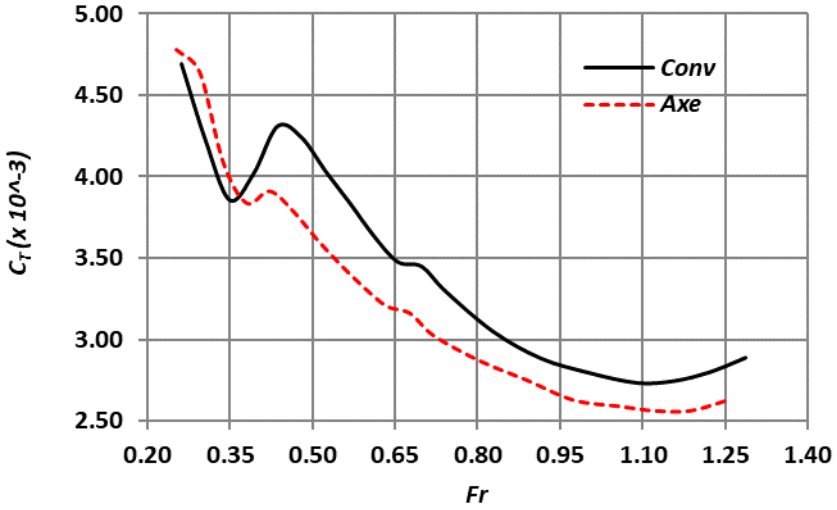

Fig. 7. Total ship resistance coefficient of conventional bow and axe bow

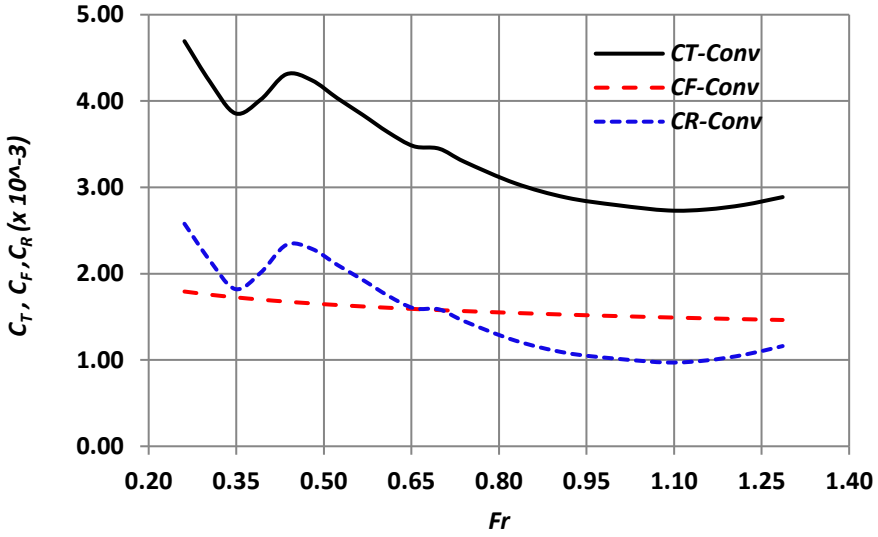

Fig. 8. Coefficient of total ship resistance (C_T), friction resistance (C_F) and residuary resistance coefficient (C_R) of conventional bow

The wave-making resistance is a key factor in this increase, with residuary resistance contributing 50% to 61% of the total resistance, consistent with findings by Lothar *et al.,* [28]. While frictional resistance is the major component of low-speed vessels' calm water total resistance, residuary resistance exceeds the frictional resistance component only at Froude numbers above 0.3.

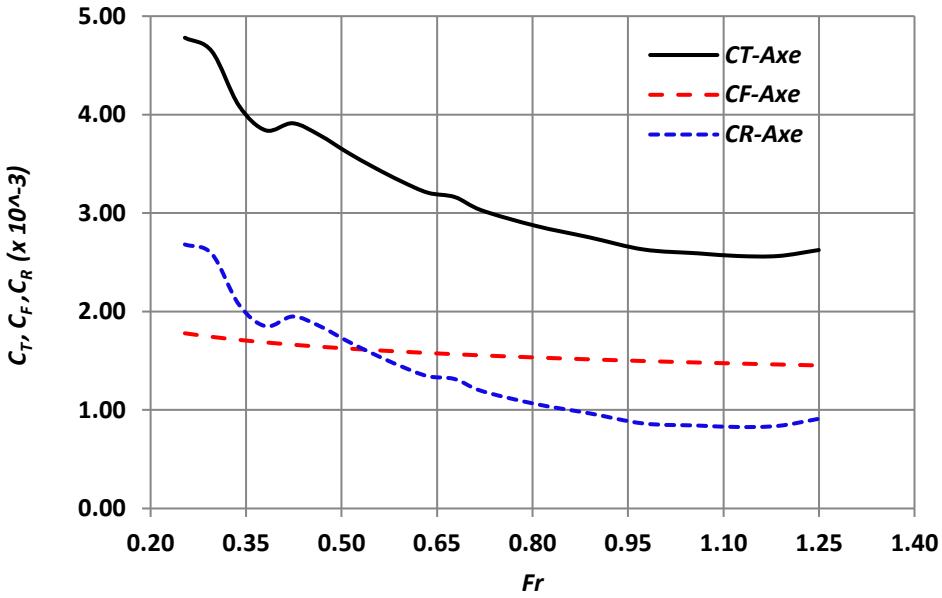

Fig. 9. Coefficient of total ship resistance (C_T), friction resistance (C_F) and residuary resistance coefficient (C_R) of Axe Bow

The wave elevation and hydrodynamic pressure characteristics at various Froude numbers for the axe bow shape are shown in Figure 10, 11, and 12. The total ship resistance for both bow shapes is proportional to the wave elevation magnitude along the hull. Figure 10(a), 11(a), and 12(a) indicate that as ship speed increases, the generated wave elevation also increases, leading to a decrease in the residuary resistance coefficient.

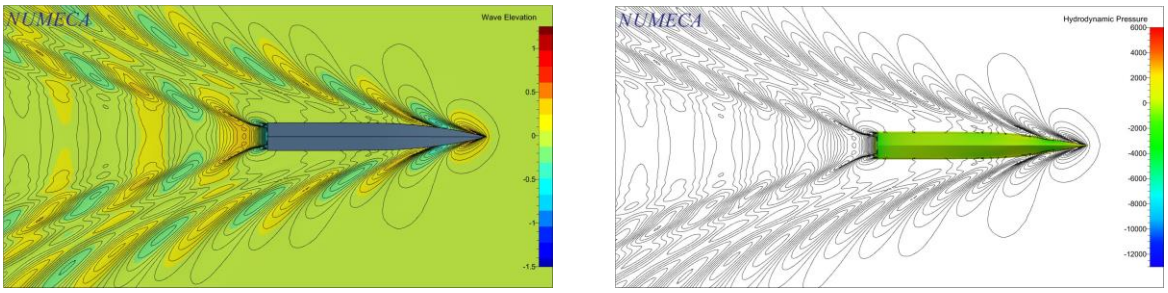

(a) (b)

Fig. 10. Visualization of wave elevation (a) and hydrodynamic pressure (b) at froude number Fr = 0.25

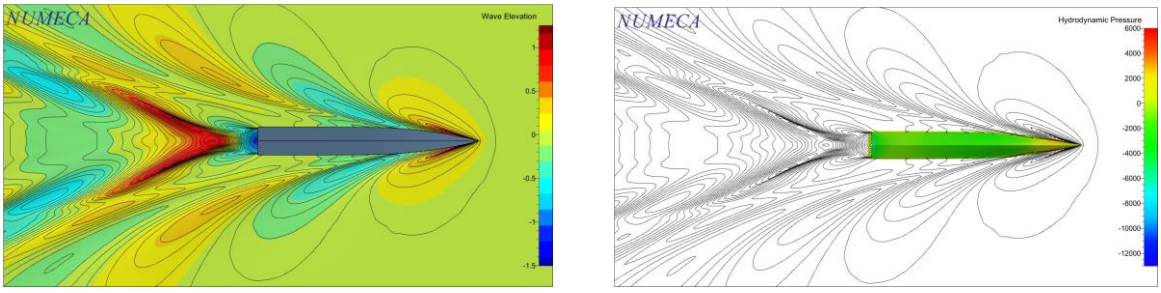

(a) (b)

Fig. 11. Visualization of wave elevation (a) and hydrodynamic pressure (b) at Froude number Fr = 0.42

The generated wave-making resistance increases due to hydrodynamic pressure, especially in the bow region. It is evident that as the Froude number increases from Fr = 0.25 to 0.60, the offset area of wave elevation also increases.. Figure 10(b), 11(b), and 12(b) illustrate that hydrodynamic pressure at the ship's bow region increases, indicated by the darker red color.

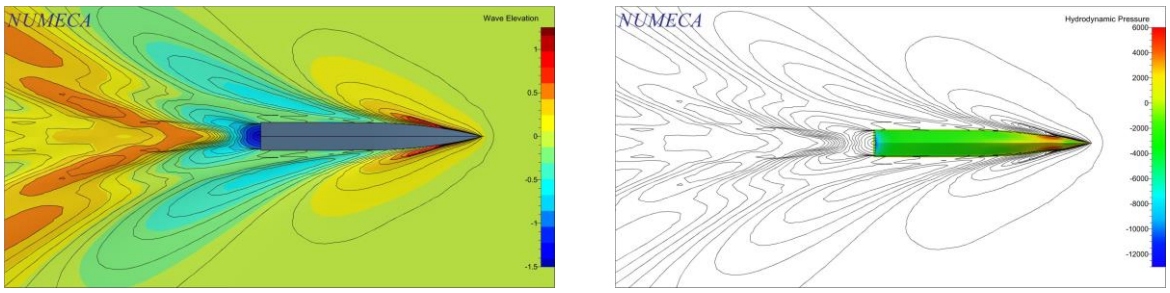

(a) (b)

Fig. 12. Visualization of wave elevation (a) and hydrodynamic pressure (b) at Froude number Fr = 0.60

3.4 Effect of Bow Hull Shape on Ship Resistance

Referring to the results of the computational investigations shown in Table 2 and Figure 6 and 7, the effect of the bow shape on the total resistance and total resistance coefficient can be defined. The tendency of the total resistance coefficient for both bow shapes is similar across the range of ship speeds. The percentage reduction of the total resistance coefficient at Froude numbers from Fr = 0.43 to Fr = 0.74, which corresponds to ship speeds from Vs = 20 knots to Vs = 32 knots, is significant, ranging from 9% to 12.4%. Notably, at Froude numbers from Fr = 0.25 to 0.35, the axe bow shape does not positively affect reducing total resistance. This indicates that the total resistance coefficient of the conventional bow shape is lower than that of the axe bow shape, being 9% lower at a Froude number of 0.3.

Additionally, obtaining the hydrodynamic characteristics through components such as residuary resistance and friction resistance is necessary. Figure 13 shows that the effect of the bow shape on frictional resistance is almost the same due to the wetted surface area being similar.

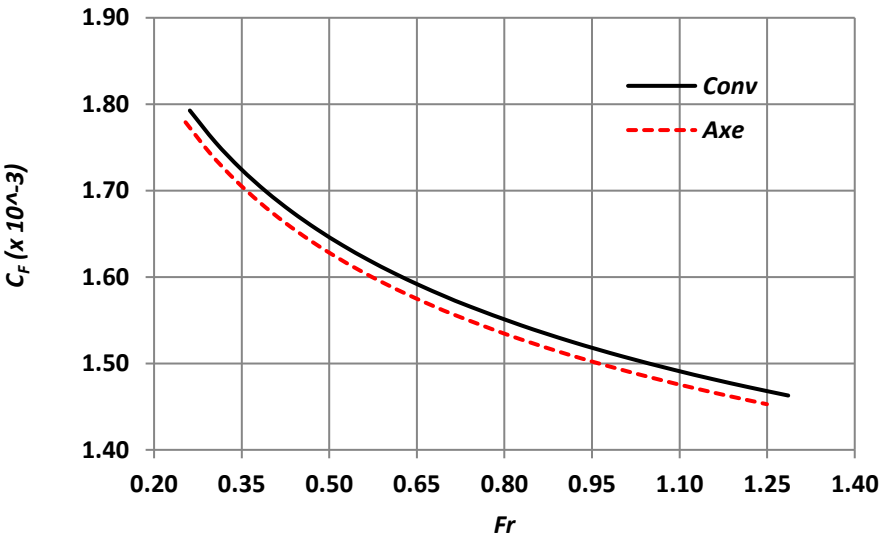

Fig. 13. Characteristic of friction resistance of conventional bow and axe bow

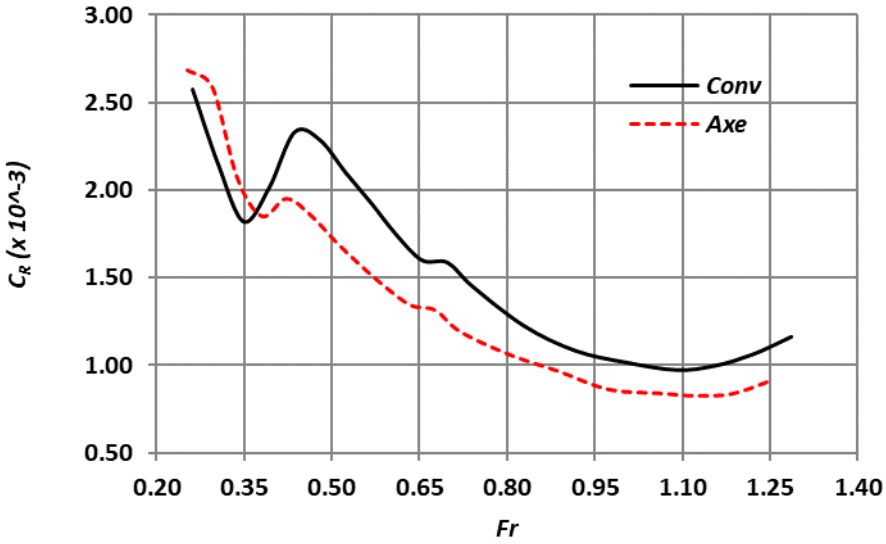

Fig. 14. Characteristic of residuary resistance of conventional bow and axe bow

However, the influence of residuary resistance on the total resistance of the two bow shapes becomes more significant, as shown in Figure 14. At Froude numbers between 0.43 and 0.74, there is a significant reduction in the residuary resistance coefficient of axe bow shape, ranging from 19% to 23%. The primary factor contributing to the rise in overall resistance at high speeds is the residuary resistance resulting from increased wave-making resistance.

The wave patterns, which primarily consist of divergent and transverse waves derived from simulations of the conventional bow shape and axe bow shape at three different ship speeds, are shown in Figure 15, 16, and 17. Figure 15(a) and 15(b) display the wave patterns at a low ship speed of Vs=14 knots. The offset area of the divergent wave near the bow region (A) and the transverse wave at the stern region (B) of the conventional bow shape is smaller, and the wave elevation is lower, as indicated by the red color, compared to the axe bow shape. This could explain why the residuary resistance coefficient of the axe bow at Fr = 0.25 to 0.35 is larger than that of the conventional bow shape.

Furthermore, as seen in Figure 16 and 17, it is essential to note that as the ship speed increases to Vs = 28 knots and Vs = 46 knots, the offset area and the red and yellow colors of the divergent wave elevation near the bow region of the conventional bow shape (A) are larger than those of the axe bow shape. Additionally, the offset area of the divergent wave at the shoulder and stern, indicated by the blue color (B), is larger for the conventional bow shape than for the axe bow shape.

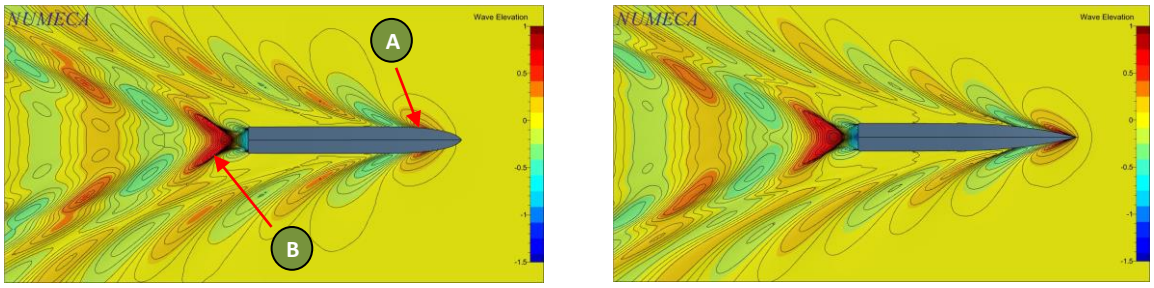

(a) (b)

Fig. 15. Wave elevation of conventional (a) and axe bow (b) at ship speed Vs=14 knot

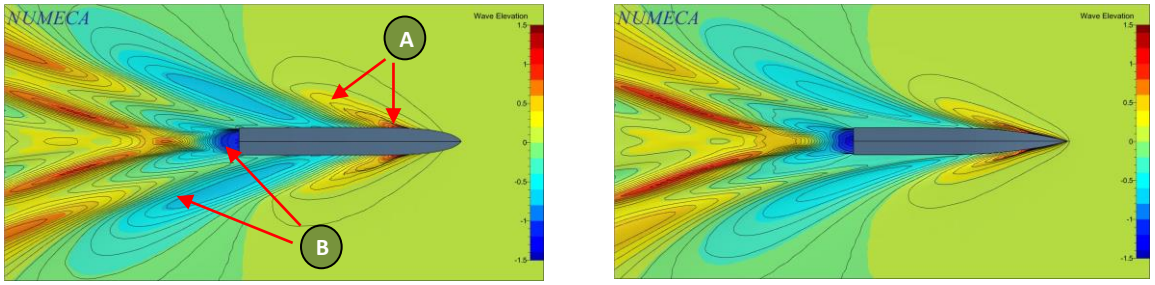

(a) (b)

Fig. 16. Wave elevation of conventional (a) and axe bow (b) at ship speed Vs=28 knots

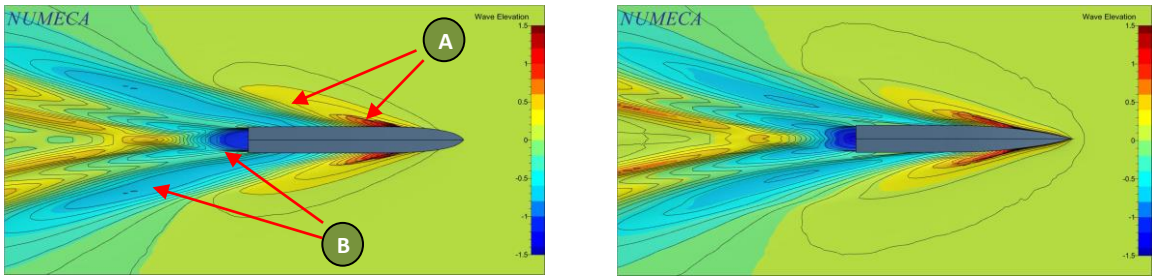

(a) (b)

Fig. 17. Wave elevation of conventional (a) and axe bow (b) at ship speed Vs=46 knots

4. Conclusion

The CFD simulation and model test approaches for the two bow shapes have been analyzed. The results provide a better understanding of the effect of bow shape on total resistance and its components. Several conclusions can be drawn, as follows:

i. The total ship resistance is proportional to ship speed; however, in this particular fast monohull, a phenomenon of a hump and a hollow appears at low Froude numbers.
ii. The simulation results show that the axe bow shape provides a significant improvement in hydrodynamic performance by reducing total resistance by up to 12.5%. This finding has been validated by ship model test results, which show good agreement.
iii. The residuary resistance of the axe bow shape has a greater influence on total resistance compared to the conventional bow, particularly at Froude numbers from Fr = 0.25 to Fr = 0.55.
iv. It was found that at low Froude numbers, from Fr = 0.25 to 0.35, the conventional bow shape has lower total resistance than the axe bow shape. This can be attributed to the smaller offset area of wave elevation in the bow and stern regions of the ship.

Acknowledgement

This study was sponsored by the Degree by Research Program of the National Research and Innovation Agency (BRIN), Indonesia, based on Decree Number 17/HK/II/2023. The author expresses sincere gratitude to the Computation Laboratory at the Department of Marine Engineering, Institut Teknologi Sepuluh Nopember (ITS), Surabaya, Indonesia, for providing the necessary resources and facilities for this study, and to the Indonesian Hydrodynamic Laboratory-BRIN for their support in conducting the model tests.

References

[1] Stopford, Martin. *Maritime economics 3e*. Routledge, 2008. https://doi.org/10.4324/9780203442661

[2] Chou, Ming-Tao, Tsung-Yu Chou, Yu-Ru Hsu, and Chi-Pao Lu. "Fuel consumption ratio analysis for transiting from various ports and harbours in Asia through the Northern Sea Route." *The Journal of Navigation* 70, no. 4 (2017): 859-869. https://doi.org/10.1017/s0373463317000078

[3] Sui, Congbiao, Peter de Vos, Douwe Stapersma, Klaas Visser, and Yu Ding. "Fuel consumption and emissions of ocean-going cargo ship with hybrid propulsion and different fuels over voyage." *Journal of Marine Science and Engineering* 8, no. 8 (2020): 588. https://doi.org/10.3390/jmse8080588

[4] Sharifi, Yaser, Hassan Ghassemi, and Hamid Zanganeh. "Various innovative technologic devices in shipping energy saving and diminish fuel consumption." *Int. J. Phys* 5, no. 1 (2017): 21-29. http://doi.org/ 10.12691/ijp-5-1-4

[5] Ibadurrahman, Ibadurrahman, A. Gunawan, and R. A. Wibowo. "Drag reduction of X-pentamaran ship model with asymmetric-hull outrigger configurations and hull separation." *Energy Reports* 6 (2020): 784-789. https://doi.org/10.1016/j.egyr.2019.11.158

[6] Kee, Keh-Kim, B-Y. Lau Simon, and K-H. Yong Renco. "Prediction of ship fuel consumption and speed curve by using statistical method." *J. Comput. Sci. Comput. Math* 8, no. 2 (2018): 19-24. https://doi.org/10.20967/jcscm.2018.02.002

[7] Bouman, Evert A., Elizabeth Lindstad, Agathe I. Rialland, and Anders H. Strømman. "State-of-the-art technologies, measures, and potential for reducing GHG emissions from shipping–A review." *Transportation Research Part D: Transport and Environment* 52 (2017): 408-421. https://doi.org/10.1016/j.trd.2017.03.022

[8] Tahara, Yusuke, Satoshi Tohyama, and Tokihiro Katsui. "CFD-based multi-objective optimization method for ship design." *International Journal for numerical methods in fluids* 52, no. 5 (2006): 499-527. https://doi.org/10.1002/fld.1178

[9] Hovland, Erlend, and Ove Tobias Gudmestad. "Trimaran concept for offshore operations in Northern Seas." In *International Conference on Offshore Mechanics and Arctic Engineering*, vol. 47470, pp. 247-256. 2006. https://doi.org/10.1115/omae2006-92211

[10] Matsumoto, Koichiro. "Development of energy saving bow shape at sea." In *Fourth Osaka Colloquium on Seakeeping Performance of Ships, October, 2000*, pp. 479-485. 2000.

[11] Gelling, Jaap L., and J. A. Keuning. "Recent developments in the design of fast ships." *Ship Science and Technology* 5, no. 9 (2011): 57-68. https://doi.org/10.25043/19098642.51

[12] Chi, Y. A. N. G., and Fuxin Huang. "An overview of simulation-based hydrodynamic design of ship hull forms." *Journal of Hydrodynamics, Ser. B* 28, no. 6 (2016): 947-960. https://doi.org/10.1016/s1001-6058(16)60696-0

[13] Huang, Fuxin, and Y. A. N. G. Chi. "Hull form optimization of a cargo ship for reduced drag." *Journal of Hydrodynamics, Ser. B* 28, no. 2 (2016): 173-183. https://doi.org/10.1016/s1001-6058(16)60619-4

[14] Zeng, Qingsong, Robert Hekkenberg, Cornel Thill, and Hans Hopman. "Scale effects on the wave-making resistance of ships sailing in shallow water." *Ocean Engineering* 212 (2020): 107654. https://doi.org/10.1016/j.oceaneng.2020.107654

[15] Fitriadhy, Ahmad, Rizuan Razali, Atiqah Yaakup, M. Ridwan Utina, Anuar Abu Bakar, Alamsyah Kurniawan, and Budianto Ontowirjo. "Computational Investigation into Predicting Total Resistance of Axe-Bow Ship's in Calm Water." *CFD Letters* 15, no. 11 (2023): 1-15. https://doi.org/10.37934/cfdl.15.11.115

[16] Ravenna, Roberto, Soonseok Song, Weichao Shi, Tonio Sant, Claire De Marco Muscat-Fenech, Tahsin Tezdogan, and Yigit Kemal Demirel. "CFD analysis of the effect of heterogeneous hull roughness on ship resistance." *Ocean Engineering* 258 (2022): 111733. https://doi.org/10.1016/j.oceaneng.2022.111733

[17] Munazid, Ali, I. Utama, and I. Ariana. "CFD Analysis onthe Development of Pre-Duct Shapeto Improve Propeller Performance." (2024). https://doi.org/10.37934/cfdl.16.2.118132

[18] Keuning, Lex JA, Serge Toxopeus, and Jakob Pinkster. "The effect of bowshape on the seakeeping performance of a fast monohull." In *TUDelft, Faculty of Marine Technology, Ship Hydromechanics Laboratory, Report 1291-P, 6th International Conference on Fast Sea Transportation, FAST2001, Southampton, UK, The Royal Institution of Naval Architects, RINA*. 2001. https://doi.org/10.3940/rina.ft.2001.21

[19] Mosaad, Mohamed A., M. M. Gafaary, Waleed Yehia, and Hussien Mohamed Hassan. "On the design of X-bow for ship energy efficiency." *Influence of EEDI on Ship Designu0026 Operation, London, UK* 22 (2017).

[20] Basil, Kunjachan T., and C. P. NajdanWaris. "Hull optimisation of fishing trawlers using ulstein x-bow and bilge keel." *International Journal of Engineering Applied Sciences & Technology* 7, no. 2 (2022): 214-220. https://doi.org/10.33564/ijeast.2022.v07i02.032

[21] Menter, Florian, and Christopher Rumsey. "Assessment of two-equation turbulence models for transonic flows." In *Fluid Dynamics Conference*, p. 2343. 1994. https://doi.org/10.2514/6.1994-2343

[22] Spalart, Philippe, and Steven Allmaras. "A one-equation turbulence model for aerodynamic flows." In *30th aerospace sciences meeting and exhibit*, p. 439. 1992. https://doi.org/10.2514/6.1992-439

[23] Deshpande, Sujay, P. Sundsbø, and Subhashis Das. "Ship resistance analysis using CFD simulations in Flow-3D." *The International Journal of Multiphysics* 14, no. 3 (2020): 227-236. https://doi.org/10.21152/1750-9548.14.3.227

[24] International Towing Tank Conference (ITTC), "*Practical Guidelines For Ship CFD Applications*". Rev.1 7.5-03-02-03 1–18. (2011)

[25] Larsson, Lars. "Ship resistance and flow." *Published by The Society of Naval Architects and Marine Engineers, SNAME, The Principles of Naval Architecture Series, ISBN: 978-0-939773-76-3* (2010).

[26] Bertram, Volker. *Practical ship hydrodynamics*. Elsevier, 2011.

[27] Molland, Anthony F., Stephen R. Turnock, and Dominic A. Hudson. *Ship resistance and propulsion*. Cambridge university press, 2017. https://doi.org/10.1017/9781316494196

[28] Lothar Bank, "Frictional Resistance", *Chapter 13 Wiley On the Library*, 2019. https://doi.org/10.1002/9781119191575.ch13